Proceedings of the 12th International Conference on
Aluminium Alloys, September 5-9, 2010, Yokohama, Japan
©2010 The Japan Institute of Light Metals
pp. 1573-1578

Microstructure and Creep Behavior of AlSiCuMgNi Piston Alloys

Shirin Ketabchi[1], Reza Mahmudi[2] and Saeed Shabestari[1]

[1] Center of Excellence for Advanced Material Processing, School of Materials and Metallurgical Engineering, Iran University of Science and Technology, Narmak, Tehran, Iran

[2] School of Metallurgical and Materials Engineering, University of Tehran, North Kargar Ave., Tehran, Iran

Creep behavior of the hypo-eutectic Al-12%Si-1.3%Cu-1%Mg-1%Ni (LM13) and hyper-eutectic Al-17%Si-1.3%Cu-1%Mg-1%Ni (LM28) piston alloys was investigated by impression creep testing. The tests were carried out under constant punching stress in the range 125 MPa to 700 MPa and at temperature in the range 490-620 K. Prior to testing, both alloys received a T6 aging treatment and were then overaged at 623 K for one hour, in order to stabilize the microstructure. Results showed that for all loads and temperatures, LM28 had a lower creep rate, and thus, a higher creep resistance than the LM13 alloy. The observed creep behaviors of the studied alloys are discussed in terms of their microstructural features.

Keywords: *Impression creep, Al-Si piston alloys.*

1. Introduction

The cast Al-Si alloys have attracted increasing attention in recent years, particularly due to the demand for lighter vehicles as part of the overall goal to improve fuel efficiencies and reduce vehicle emissions [1, 2]. Hypoeutectic Al-Si alloys have long been used in the moderately high temperature regimes, while hypereutectic Al-Si alloys have generally received little attention due to the presence of very hard primary Si particles that reduce their machinability [3]. However, there is a growing interest in hypereutectic Al-Si alloys for their superior wear resistance, low thermal expansion coefficient, and high corrosion resistance. Due to economic and environmental requirements, it is becoming increasingly important to extend engine efficiency. One of the common procedures to achieve this goal is increasing the engine's performance temperature. At high working temperatures, creep which is the strain response of the material to a constant stress over a period of time becomes prominent. This process can lead to the degradation of engine performance, and thus it is quite desirable to improve the creep resistance of the employed materials.

Although, an extensive amount of information is available on the wear and fatigue behavior of Al-Si alloys, the published data on the creep properties of these alloys are rather rare. The creep characteristics of hypo-eutectic and near-eutectic Al-Si cast alloys have been considered and often compared with those of the short fiber reinforced base alloys [4]. Spigarelli et al. [3, 5] studied the creep behavior hyper-eutectic Al-Si alloys by conventional tensile creep tests. They showed that the creep curves exhibited a short primary region, followed by a minimum creep rate range and by a long tertiary stage. The microstructural analysis suggested a similarity between the creep of the Al-Si alloy and Al-matrix discontinuously reinforced composites.

The impression creep of cast Al-Si alloys has not been studied previously. Therefore, the aim of this study is to investigate impression creep properties and the major creep deformation mechanisms of LM13 and LM28 alloys using the impression testing technique, which has been widely used in the creep study of different materials [6-10]. This method involves the time dependent penetration of a cylindrical punch with a flat end into the material under constant load and temperature. During the test, variation in penetration depth of the impresser with time is continuously recorded, and thus the penetration rate or impression velocity can be obtained. These tests have proved to yield very similar results to those obtained by the conventional creep tests [11, 12].

2. Experimental Procedure

2.1 Materials and processing

Pure Cu, Ni, Mg, and Si together with Al-10Sr, Al-10Zr, Al-5Ti-1B, and Cu-15P master alloys were used to prepare the required compositions from a commercial LM13 ingot. Melting was carried out in a graphite crucible placed in an electrical resistance furnace at 1050 K. Both alloys were solution-treated at 783 K for 8 hours followed by quenching in water and artificial aging at 448 K for 8 hours. They were then overaged at 573 K for one hour, in order to stabilize the microstructure. The heat-treated samples were studied by scanning electron microscopy (SEM) to examine the aging-treated microstructure as well as the evolution of microstructure after creep. Etching was carried out using a 1% hydrofluoric acid etchant at room temperature. Energy-dispersive spectroscopy (EDS) analysis was performed to reveal the composition of different phases in different areas of the microstructure. Some specimens after creep were cut parallel to the loading direction in order to study the microstructure evolution in the deformation zone beneath the indenter.

2.2 Impression creep tests

The cast bars were cut into 4-mm slices and tested in an impression tester. The details of the testing arrangement are explained elsewhere [7] and will only be briefly described here. A SANTAM-STM 20 universal tensile testing machine equipped with electric furnace was used to perform constant-load impression tests. A flat-ended cylindrical punch of 2 mm diameter was mounted in a holder positioned in the center of vertical loading bar. The specimen was located on an anvil below the loading bar; the assembly of the specimen and the indenter was accommodated by the split furnace. The tests were performed in the temperature range 490 to 620 K, and under applied stresses in the range 125 to 700 MPa for dwell times of up to 4000 seconds. After application of the load, the impression depth was measured automatically as a function of time by the machine and the data were acquired by a computer.

3. Results and Discussion

The SEM micrograph of the LM13 alloy, shown in Fig. 1a, indicates that the microstructure consists of relatively fine eutectic Si (dark phase) and coarse acicular β-phase (white phase) distributed in the α-Al matrix. Fig. 1b shows the EDS analysis of the bright β-phase, indicating that, Al, Fe, Si, Ni, Mn, and Cu are the main constituents of the microstructure.

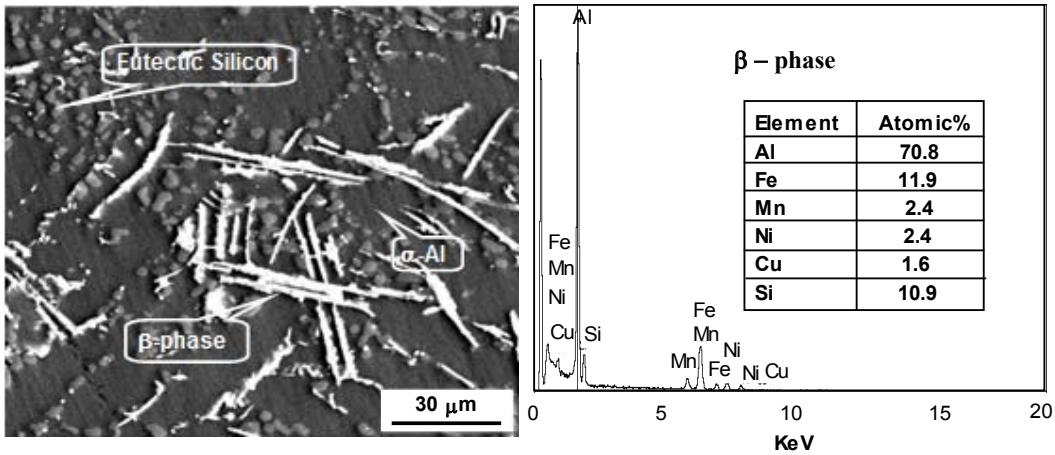

Fig. 1. (a) SEM micrograph of LM13, showing the distribution of eutectic Si and acicular β-phase in the α-Al matrix, and (b) EDS analysis of the β-phase particles.

For comparison, the SEM micrograph of the LM28 alloy is depicted in Fig. 2a. The microstructure of this hyper-eutectic alloy consists of fine eutectic Si, coarse blocky primary Si, and irregularly-shaped intermetallic-phase in the α-Al matrix. The quantitative analysis of the intermetallic phase is shown in Fig. 2b. Similar to the LM13 alloy, these particles contain Al, Fe, Si, Ni, Mn, and Cu. However, their morphology has changed from coarse acicular to fine irregular-shape.

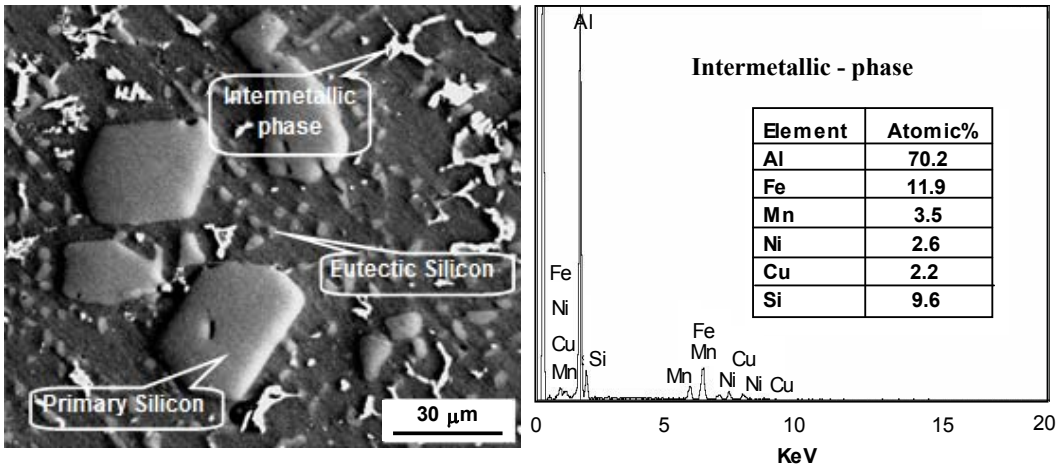

Fig. 2. (a) SEM micrograph of LM28, showing the distribution of fine eutectic Si, coarse blocky primary Si, and irregularly-shaped intermetallic-phase in the α-Al matrix, and (b) EDS analysis of the intermetallic-particles.

Typical penetration depths of the punch as a function of time under different stress levels for both LM13 and LM28 alloys tested at 570 K are shown in Fig. 3. As can be seen, although each of the individual impression curves does not always exhibit a pronounced primary creep stage, they all eventually show a relatively long secondary or steady-state region where depth increases linearly with time. Since the impression test is compressive in nature, fracture of the specimen does not occur, and hence, it is obviously not possible to record a third stage of the curve, as opposed to what occurs in an ordinary creep test.

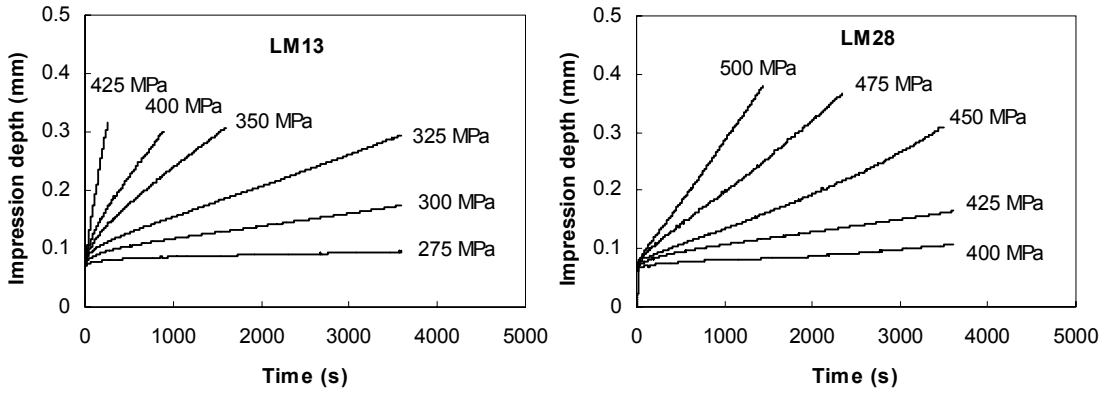

Fig. 3. Impression creep curves obtained at 570 K under different punching stresses for the LM13 and LM28 alloys.

Impression creep tests were carried out at different temperatures and under different stress levels for both materials. The steady-state or minimum creep rates were then determined by plotting the derivative of impression depth against impression depth. The obtained minimum creep rates are plotted under different constant stress levels at 490, 530, 570 and 620 K, as shown in Fig. 4. It can be observed that, at all testing temperatures and under all stress levels, the minimum creep rates of the LM28 are much lower than those of the LM13 alloy.

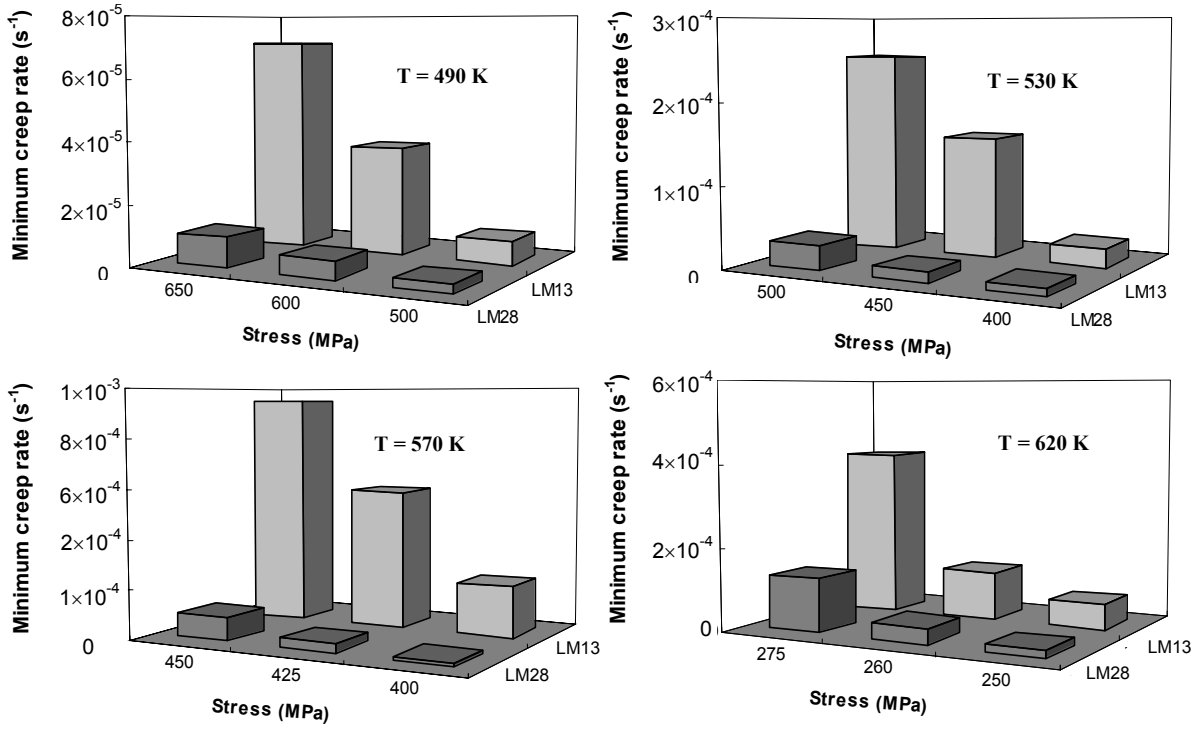

Fig. 4. Comparison of minimum creep rates obtained at different punching stresses for the materials tested at four different temperatures.

The observed difference in the impression creep behavior of the alloys can be attributed to their microstructural evolution during impression creep. Accordingly, some crept samples were sectioned along the impression direction in the middle of the impressed area and the microstructure was studied beneath the indenter. Fig. 5a illustrates the microstructural evolution of LM13 in the vicinity of the edge of impression after creep testing at 570 K. As can be observed, there are three distinguishable regions separated from each other by curved lines. No microstructural changes are detectable in the dead zone region immediately below the indenter that is not deformed during creep test. Adjacent to this zone, there exists a severely deformed region, in which the strained and broken particles are aligned in the direction of material flow. These particles, which trace the direction of deformation, are shown in Fig. 5b at a higher magnification. From this picture, it is evident that particles are strained along the deformation path and are broken as a result of severe plastic deformation. This effect can be ascribed to the extensive shear deformation taking place below the indenter. The observed substantial deformation could be due to possible softening of the matrix and also to the fracture of long acicular β-phase particles, which cannot impede plastic deformation and easily deform with developing shear stresses.

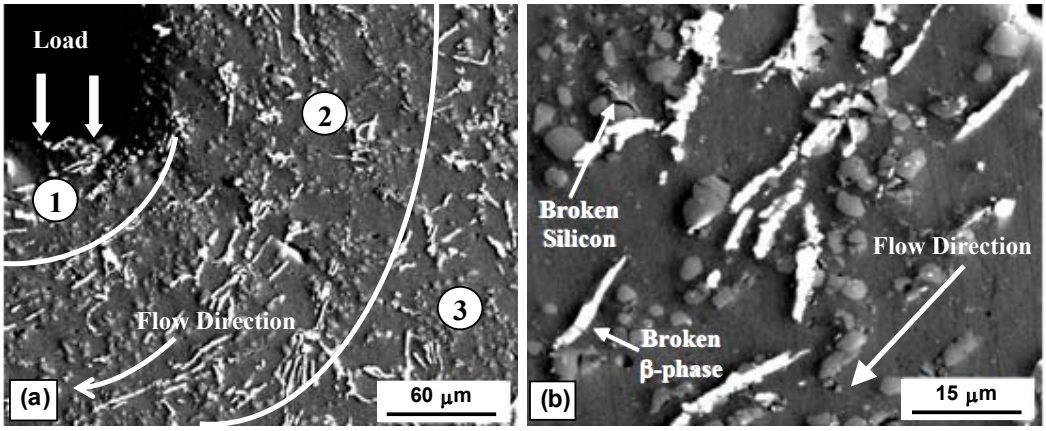

Fig. 5. (a) Cross section of the impression edge in LM13 at 570 K, showing the flow in deformation zone 2, and (b) a higher-magnification view showing the broken particles along flow direction in the deformation zone.

In contrast to the behavior of LM13, the microstructure of the LM28, shown in Fig. 6a, contains a rather uniform distribution of the primary Si particles and the intermetallics with almost no distinct flow pattern in region 2. A closer view of the deformation zone, depicted in Fig. 6b, indicates that some of the coarse primary silicon particles are cracked and fractured under the applied load. Despite this particle fragmentation, the material exhibits superior creep properties, as compared with the LM13 alloy. This can be attributed to the high thermal stability and strength of the microstructural constituents, which resists the applied shear stresses in the deformation zone at high temperatures. The lower creep rate, and thus higher creep resistance of the LM28 alloy is a direct consequence of this stability and strength. The achieved strength is caused by the presence of the hard primary Si particles, which act as the hard ceramic particles in metal matrix composites. This composite strengthening effect makes the deformation of the material more difficult under the applied punching load. Furthermore, the fine intermetallic particles can resist the shear deformation in the deformation zone and improve the overall creep resistance of the alloy.

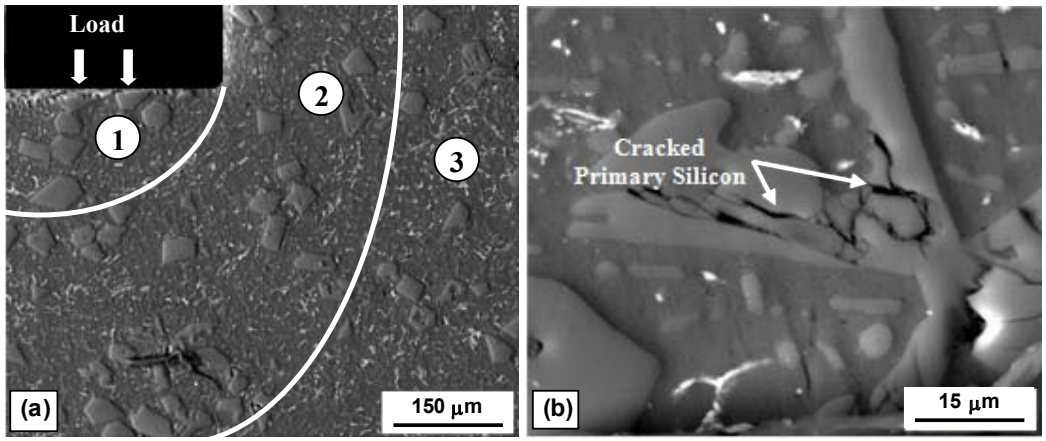

Fig. 6. (a) Cross section of the impression edge in LM28 at 570 K, showing no distinct flow pattern under the punch, and (b) a higher-magnification view showing the cracked particles in the deformation zone.

4. Conclusions

The impression creep characteristics of the hypo-eutectic Al-12%Si-1.3%Cu-1%Mg-1%Ni (LM13) and hyper-eutectic Al-17%Si-1.3%Cu-1%Mg-1%Ni (LM28) piston alloys investigated in the temperature range 490 to 620 K under stress levels in the range of 125 MPa to 700 MPa yielded the following conclusions:

1. The structure of LM13 consisted of fine eutectic Si and the coarse intermetallic acicular β-phase distributed in the α-Al matrix. The high aspect ratio of this phase made it prone to fracture under the punching load during creep testing. The creep resistance of the LM13 alloy was thus adversely affected by the low strength of this phase, which could not resist the applied load. The deformation zone under the punch in this alloy showed a clear flow pattern, with the broken particles being aligned in the flow direction.

2. In the LM28 alloy, the coarse block-shaped primary Si particles coexisted with the intermetallic phase having an irregular morphology. The thermally stable hard bulky Si particles together with the finely distributed intermetallics strengthened the α-Al matrix. The role of Si particles is similar to that of the hard ceramic particles in the metal matrix composites. These two effects resulted in enhanced creep resistance of the LM28 alloy, as compared to that of LM13.

References

[1] P. Sepehrband, R. Mahmudi and F. Khomamizadeh: Scripta Mater. 52 (2005) 253–257.
[2] R. Mahmudi, P. Sepehrband and H.M. Ghasemi: Mater. Lett. 60 (2006) 2606–2610.
[3] S. Spigarelli, M. Cabibbo, E. Evangelista and S. Cucchieri: Mater. Letts. 56 (2002) 1059– 1063.
[4] G. Requena and H.P. Degischer: Mater. Sci. Eng. A 420 (2006) 265–275
[5] S. Spigarelli, E. Evangelista and S. Cucchieri: Mater. Sci. Eng. A 387–389 (2004) 702–705.
[6] A. Rezaee-Bazzaz and R. Mahmudi: Mater. Sci. Technol. 21 (2005) 861–866.
[7] R. Mahmudi, A.R. Geranmayeh and A. Rezaee-Bazzaz: J. Alloys Compd. 427 (2007) 124-129.
[8] R. Mahmudi, A.R. Geranmayeh, H. Noori, N. Jahangiri and H. Khanbareh: Mater. Sci. Eng. A 487 (2008) 20–25.
[9] F. Kabirian and R. Mahmudi: Metall. Mater. Trans. A 40A (2009) 116–127.
[10] R. Mahmudi, A. Karsaz, A. Akbari-Fakhrabadi and A.R. Geranmayeh: Mater. Sci. Eng. A 527 (2010) 2702–2708.
[11] R. Mahmudi, A. Rezaee-Bazzaz and H.R. Banaie-Fard: J. Alloys Compd. 429 (2007) 192–197.
[12] C. Park, X. Long, S. Haberman, S. Ma, I. Dutta, R. Mahajan and S.G. Jadhav: J. Mater. Sci. 42 (2007) 5182–5187.